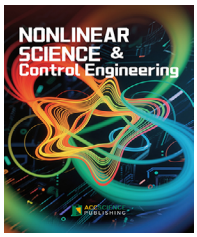
Contents lists available at AccScience Publishing
Nonlinear Science and Control Engineering (NSCE)
Vol. 2, No. 3 (2026)
https://accscience.com/journal/nsce



A comparative study of load frequency control using advanced controllers and digital deadbeat control with signal stabilization for limit cycle mitigation

Kartik Chandra Patra* and **Asutosh Patnaik**

Department of Electrical Engineering, Faculty of Engineering and Technology, C. V. Raman Global University, Bhubaneswar, Odisha, India

Article History:
Received: June 6, 2026
Revised: August 13, 2026
Accepted: September 9, 2026
Published online: September 28, 2026

A B S T R A C T

In interconnected power systems, inadequate power generation relative to contracted load demand and continuously varying electrical loads can cause frequency instability and power imbalance. Therefore, effective monitoring and coordinated control strategies are essential to preserve system reliability and prevent potential disturbances. One widely adopted approach is tie-line bias control, which regulates scheduled system frequency and tie-line power flow by computing the area control error (ACE). ACE combines frequency deviation and tie-line power mismatch and is used to automatically optimize generator output, ensuring a continuous balance between generation and demand. This enables each control area to contribute fairly to overall grid stability while facilitating coordinated power exchange among interconnected regions. However, load variations in any area can propagate throughout the interconnected network, causing frequency deviations and tie-line power instabilities that must be minimized. Load frequency control (LFC) addresses this bottleneck by utilizing ACE as a feedback signal. Conventional LFC systems typically consist of turbine, generator, and governor dynamics and often exhibit backlash nonlinearities. These nonlinearities can generate self-sustained oscillations/limit cycles under autonomous operation, degrading frequency regulation performance and tie-line power control. To address this limitation, this study uses a signal stabilization technique employing Gaussian or deterministic signals to mitigate limit cycles. Subsequently, a digital deadbeat controller is applied to accomplish quick and accurate frequency regulation. The main objective is to drive ACE toward zero, thereby restoring frequency deviation and tie-line power errors to their desired values.

Keywords: Load frequency control; Tie-lines; Automatic generation control; Limit cycles; Area control error

CC BY

1. Introduction

The basic objective of an integrated multi-area power system is to supply electric power to every consumer with good quality, stability, and reliability at steady state. Load frequency control (LFC) faces major challenges from renewable energy integration, low system inertia, complex load variations, and stochastic load demands. These factors disrupt the balance between power generation and demand, causing severe frequency instabilities. The principal challenges are renewable intermittency and

***Corresponding author:**
Kartik Chandra Patra (kcpatra@cgu-odisha.ac.in).

Citation: Patra KC, Patnaik A. A comparative study of load frequency control using advanced controllers and digital deadbeat control with signal stabilization for limit cycle mitigation . *Nonlinear Sci Cont Eng*. 2026;2(3):026230021. doi: 10.36922/NSCE026230021

Copyright: © 2026 The Author(s). This is an Open Access article distributed under the terms of the Creative Commons Attribution License, permitting distribution, and reproduction in any medium, provided the original work is properly cited.

stochastic load demands. Under such scenarios, LFC, or automatic generation control (AGC), is a vital operation used in power systems to maintain power balance between interconnected areas and control power flow in tie lines. The demand for electric power is increasing, threatening fossil fuel depletion and increasing environmental pollution; the shift toward green energy is inevitable and crucial.

In the current scenario, deploying renewable energy sources (RESs) is indispensable; they are now actively integrated into the power grid and regarded as a promising solution.[1] Furthermore, power system interconnections continue to expand in both scale and complexity, extending from multi-grid integration to the development of regional, provincial, and even global energy networks.[2,3]

Electrical power cannot be stored in huge quantities.[4] Therefore, electricity production must continuously match consumption. Moreover, owing to their intermittent nature and limited inherent redundancy, RESs can introduce instability into the power system.[5] The micro-grids are created by RESs and located in different areas. Therefore, the concepts of production and consumption mostly apply to RESs.

We can consider the main grid, or national grid, as a single vast interconnected network. Several challenges and responsibilities must be addressed to ensure power system stability, reliability, and quality.[5]

To meet these objectives, the simple, easy-to-implement, robust, economical, and widely used decentralized control configuration is an age-old practice in LFC for interconnected power systems, aiming to achieve stable system frequency and power balance between areas.[6]

The TBC technique is extensively employed in LFC for multi-area interconnected systems. It maintains system frequency and tie-line power at their scheduled values.[7] It calculates a control signal called area control error (ACE), which combines frequency deviation (Δf) and tie-line power flow deviation (ΔPL), and then uses this error to automatically adjust generator output. This ensures that each power system area contributes to maintaining grid stability without imposing an excessive regulating burden on its neighbors.[8-16]

Previous studies[17-18] clearly state that limit cycle (LC)/ self-sustained oscillations due to backlash nonlinearity in the governor must be avoided for proper LFC performance. This indicates a basic requirement to mitigate/quench LC, which has been addressed in other studies.[19-22]

To capture the effect of RESs on the system, a first-order transfer function is adopted, where the transfer function gain corresponds to the RES penetration level.[23] Changes in wind turbines, generators, solar irradiance, and solar power output have been taken into account.[24] The increasing penetration of RESs may pose challenges to power system stability, thereby increasing the complexity of control and stabilization.[25]

Whether LFC or AGC, these operations occur continuously to maintain power system stability. Its fundamental function is to maintain the balance between interconnected areas by regulating Δfs and tie-line power flows. In distributed grid systems incorporating microgrids and RESs, LFC ensures effective power sharing and coordinated operation among interconnected areas, thereby enhancing overall system reliability and stability.[26,27]

This study explores recent developments in LFC and highlights prospective research directions for interconnected multi-area power systems (IMAPSs). Gulzar *et al.*[28] conducted a comprehensive literature review and presented many noteworthy works. Khan *et al.*[29] discuss and critically highlight how, over the past decade, the conventional power system has progressively transformed into a highly interconnected, digitally enabled, and renewable-rich energy ecosystem. They cite a few models with advanced controllers. Before discussing these two articles, we highlight key points from Gulzar *et al.*[28] The most recent advancement in LFC primarily aims to mitigate/quench frequency oscillations and ensure stable operation of IMAPSs. This work provides a comprehensive overview, covering both traditional control methods and recent advancements in technologies and methodologies. It evaluates various control strategies, including robustness and adaptive controller properties, fuzzy control techniques, and a range of optimization approaches—both classical and modern—applied to LFC in IMAPSs. The assessment emphasizes recent technological progress and advanced control tactics. Furthermore, the article delivers an in-depth analysis of the limitations and challenges of LFC in modern interconnected power systems. Finally, it thoroughly explores future strategies and solutions to address increasing system complexity and operational inefficiencies.

In recent years, electrical power has become an essential commodity, and an uninterrupted supply is critical to meeting societal needs, enabling industrial productivity, and supporting economic progress. A resilient power system can withstand and adapt to disruptions, fluctuations, and varying load demands. The stochastic and dynamic nature of power system loads causes demand fluctuations that directly affect system frequency and lead to deviations in tie-line power from nominal levels. To meet the rising power demand, power systems are increasingly interconnected across multiple generating regions, enabling them to serve high-demand areas more effectively. However, in such an interdependent network, system disturbances initiated in one area can disrupt the entire power supply. Therefore, maintaining frequency stability is paramount. AGC returns the system to its nominal steady-state condition by regulating generation levels and balancing power generation with load demand. This process stabilizes both frequency and tie-line power flows, a function known as LFC. LFC thus plays a critical role in safeguarding power system stability.

In the current context, LFC can be viewed through a modern technological lens, alongside the traditional strategies discussed earlier. This study aims to provide a detailed examination to support future scholarly

investigations by incorporating the latest methods and technologies used in frequency control. We will present examples of innovative and feasible approaches to addressing LFC challenges in intelligent and interconnected power networks, including systems integrating thermal energy, RES, and IMAPSs. It subsequently provides a comprehensive assessment of the current status of LFC, highlights prevailing challenges and limitations, and suggests promising avenues for future research.[28]

In Tavakoli *et al.*[30], a novel intelligent tilted integral derivative–intelligent controller for LFC in multi-area, multi-source interconnected power systems by integrating brain emotional learning with tilted integral derivative control is proposed for the first time, with controller parameters optimally tuned using the equilibrium optimizer (EO) to achieve enhanced dynamic performance and robustness under nonlinearities, parameter uncertainties, communication delays, load disturbances (ΔPLs), and renewable energy variability.

Simulation studies on a two-area multi-source power system comprising thermal, gas, hydro, wind, and solar generation demonstrate that the proposed tilted integral derivative–intelligent controller significantly outperforms conventional proportional–integral–derivative (PID) and other advanced controllers by reducing Δfs, improving robustness, lowering performance indices, and providing superior disturbance rejection, highlighting its potential for reliable and efficient operation of modern renewable-integrated smart power grids.

The AGC framework consists of two fundamental control mechanisms: the automatic voltage regulator (AVR) and LFC. The AVR maintains voltage stability, whereas the LFC supervises load demand variations and mitigates Δfs. By balancing generation and demand, LFC ensures zero steady-state error (SSE) and preserves the scheduled frequency and tie-line power interchange among interconnected control areas.[31-34]

The AVR maintains voltage stability and enhances power system reliability by regulating generator excitation voltage in response to load fluctuations.[35–39] LFC is implemented through three control layers, namely primary, secondary, and tertiary control. Primary control serves as the first line of defense against load perturbations by restoring the balance between generation and demand. This control action is primarily achieved through the turbine governor, which regulates generator speed and responds rapidly to frequency variations.[40,41]

When the primary control response is insufficient to correct Δfs, the secondary control system activates to restore frequency to its nominal operating point and maintain system stability. This system manages power flow among interconnected areas by adjusting the output of individual turbine units.[42–44] When necessary, the tertiary control, also commonly termed the manual frequency restoration reserve, can be engaged by the operator. This level is typically used to replenish the secondary reserve in cases of severe generation or load drops.[45,46]

Many researchers have approached the LFC problem using linearized models,[47,48] despite the inherently large-scale and nonlinear nature of power systems. Subsequent studies developed power system models—both continuous and discrete—that incorporated generation rate constraints.[49–51] These investigations also considered the dynamic behavior of power systems and employed optimal tracking methods to address the LFC challenge.[52]

Researchers have extensively studied nonlinearities in contemporary power networks, particularly the dynamic effects of governor deadband (GDB) or backlash on governor and supplementary-controller performance.[53,54] It has been emphasized that the speed governor is a key component in maintaining effective system speed regulation. Studies have shown that GDB or backlash induces area frequency and tie-line power oscillations, negatively impacting system responsiveness.[55]

The proposed work focuses on the latest advancements in LFC; the research aims to examine the current state and establish a framework for future progress in IMAPSs. LFC primarily aims to reduce frequency instabilities, improving system performance and ensuring stable IMAPS operation. This study presents a comprehensive comparison of conventional control schemes and state-of-the-art technologies, highlighting the evolution of modern control methodologies. It also examines different control strategies, robustness, and the adaptive properties of LFC controllers for IMAPSs. A vivid, comprehensive study has been made through four suitable models selected from Khan *et al.*[29] and one most suitable model selected from Tavakoli *et al.*[30]

The rest of this article is structured as follows. Section 1 introduces the topic and provides a comprehensive review of existing research. Section 2 describes and explains how TBC works. Section 3 selects an appropriate model that can achieve the goal proposed in the article and tests different models using a step response. Section 4 estimates LC in all models due to backlash nonlinearity. Section 5 presents a complete mitigation of LC by using a signal stabilization method that incorporates both deterministic and random excitation signals,[22,56–58], where synchronization of the forcing signals is observed. Section 6 presents the application of digital control with a deadbeat approach.[59–61] As a result, all models exhibit transient-free and ripple-free behavior while achieving zero steady-state error, with the response occurring in the least time. Thus, the study thoroughly investigates future strategies and approaches to enhance LFC performance and stability amid increasing system complexity and uncertainty.

The rapid integration of electric vehicles introduces substantial charging demand and vehicle-to-grid capabilities, posing new challenges for LFC due to increased variability and uncertainty in power system operation. Consequently, advanced LFC strategies must intelligently coordinate EV charging and discharging with conventional generation to maintain frequency stability, ensure real-time power balance, and enhance the reliability and resilience of modern power systems, making electric

vehicles a promising solution for addressing the operational challenges of future power distribution networks.[62]

2. Tie-line bias control applicable to load frequency control for multi-area interconnected systems

The conventional TBC framework method is widely employed in LFC for multi-area interconnected systems. This method helps maintain both system frequency and power flow across interconnecting tie lines at their scheduled values. It operates by calculating the ACE, defined as in **Equation 1:**

$$ACE = \Delta P_{tie} + B\Delta f \quad (1)$$

where ΔP_{tie} is the deviation in scheduled tie-line power interchange from its scheduled value, Δf is the deviation of the area's frequency from its nominal value, and B is the area's frequency bias constant, a factor representing the sensitivity of its frequency response to load changes. The ACE was used to generate control signals that adjust the outputs of generators in that area. The primary goal is to drive the ACE toward zero, which simultaneously returns both frequency and tie-line power flow to their desired, stable values.

2.1. Analytical investigation of power loss changes under frequency deviation conditions

This section presents an analytical evaluation of power loss variation with respect to Δf. A non-zero Δf indicates an inherent imbalance in the interconnected system, which can manifest as additional losses in generation, transmission, or load components.[7] **Figure 1** depicts the relationship between the measured Δf and ΔPL. The model incorporates the output power deviations of multiple generating units, denoted by ΔP_{m1}, ΔP_{m2}, …, ΔP_{mn}. The dynamic behavior of the system is represented through the equivalent inertia constant (M_{eq}) and the damping coefficient (D). This modeling approach facilitates the design of robust LFC strategies and enhances overall system stability and performance.

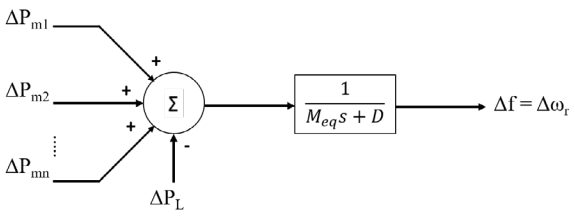


Figure 1. Block diagram representation of the load frequency control (LFC) system showing the combined effect of load variation (ΔP_L) and generator power output deviations (ΔP_{m1}, ΔP_{m2}, …, ΔP_{mn}) on frequency deviation (Δf), modeled through the equivalent inertia (M_{eq}) and damping (D) dynamics[7]

When the system load increases by ΔP_L, generated power initially falls below demanded power, causing the system frequency to decrease. The turbine governors of all interconnected generating units detect this frequency reduction and increase their mechanical power output according to their respective speed regulation (droop) constants Ri[7]. Simultaneously, many electrical loads exhibit frequency-dependent characteristics, represented by the load damping coefficient, D, whereby a reduction in frequency naturally decreases the power consumed by certain loads (e.g., induction motors).

The steady-state Δf resulting from the combined effects of governor action and load damping is expressed as **Equation 2**:

$$\Delta f = \frac{-(P_L)}{\left(1/R_1 + 1/R_2 + 1/R_3 \ldots + 1/R_n\right) + D} = \frac{-P_L}{1/R_{eq} + D} \quad (2)$$

where, $R_{eq} = \dfrac{1}{1/R_1 + 1/R_2 + \ldots + 1/R_n}$

The parameter R, commonly known as the governor speed regulation or droop characteristic, quantifies the relationship between the change in system frequency (or speed) and the corresponding change in generator power output. It is defined as the percentage change in speed (or frequency) divided by the percentage change in power output and can be expressed as **Equation 3**:

$$R\% = \frac{\text{Percentage change in frequency}}{\text{Percentage change in output power}} \times 100 = \frac{\omega_{NL} - \omega_{FL}}{\omega_0} \times 100 \quad (3)$$

where ω_{NL} is the steady-state speed at the no-load condition, ω_{FL} is the steady-state speed at the full-load condition, and ω_0 denotes the nominal (rated) speed of the generator. The droop characteristic plays a crucial role in load sharing among parallel generators and in maintaining system frequency stability. **Equation 3** quantifies how much system frequency changes when generator output shifts from no-load to full-load conditions.

Figure 2 shows the speed regulation (droop) characteristics of generating units used in LFC. Curve 1 represents the ideal linear frequency–power relationship assumed in theoretical analysis, whereas Curves 2 and 3 illustrate the actual characteristics of steam and hydraulic generating units, respectively, which exhibit slight nonlinearities due to turbine-governor dynamics and practical operating constraints. The negative slope indicates that system frequency decreases as generator output increases. These droop characteristics enable automatic load sharing among interconnected generating units and form the basis of primary frequency control in power systems.

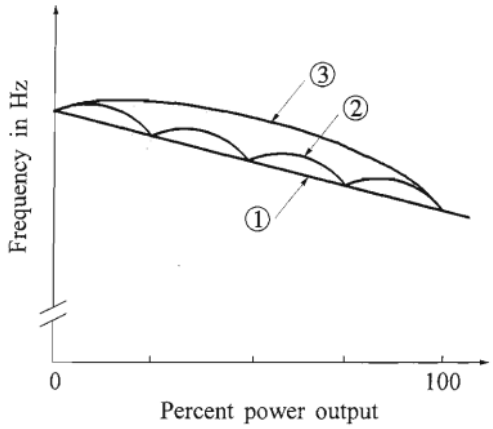


Figure 2. Governor droop characteristics showing the relationship between system frequency and generator power output. Curve 1 represents the ideal linear droop characteristic, Curve 2 illustrates the actual characteristic of steam turbine generating units, and Curve 3 depicts the actual characteristic of hydraulic generating units. The nonlinear nature of practical governor responses causes deviations from ideal linear behavior over the operating range.

3. Step response of different models

Figure 3 depicts the model structure and signal flow diagram reported in Khan *et al.*[29], developed employing the MATLAB Simulink Toolbox (MATLAB 9.2.0.538062 [R2017a]). The model includes the governor, turbine, and generator units interconnected in cascade. A PID-based LFC strategy, as stated in Khan *et al.*[29], was employed to regulate the system frequency. **Figure 4** illustrates the equivalent step response after a sudden ΔPL. The Δf steadily decreases over time and settles to its steady-state value (Δf = 0) within 20 s, demonstrating effective mitigation of transient oscillations and a successful return to nominal operating conditions.

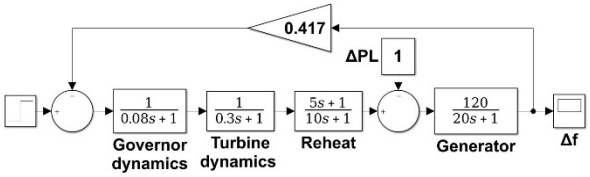


Figure 3. Block diagram of a single-area load frequency control (LFC) system incorporating governor, turbine, reheat stage, power system dynamics, and droop characteristics for frequency regulation under load disturbances

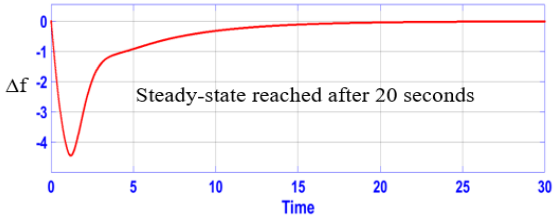


Figure 4. Frequency deviation (Δf) response of the single-area load frequency control system following a step load disturbance, showing an initial undershoot and gradual recovery to steady state within approximately 20 s

Figure 5 presents the model structure of the GDB and generation rate constraint reported in Khan *et al.*[29] **Figure 6** shows the equivalent step response following the ΔPL. The result shows that Δf progressively diminishes and reaches its steady-state value (Δf = 0) within 20 s, indicating the end of the transient period and the system's successful recovery to its nominal operating frequency.

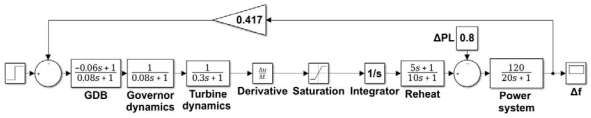


Figure 5. Block diagram of single-area load frequency control (LFC) system incorporating a thermal generator with generation rate constraint (GRC) and governor deadband (GDB) nonlinearities

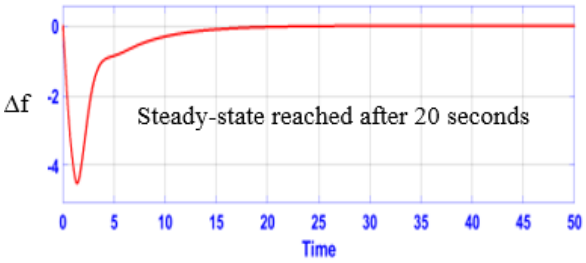


Figure 6. Results showing the system step response reaching steady state (Δf = 0) after 20 s, once the transients subside

The system's dynamic behavior was assessed by investigating the step response in the developed model under a ΔPL. The model comprised governor, turbine, and generator elements and was initially developed without backlash nonlinearity to maintain linearity. A disturbance was introduced, and the resulting Δf was monitored. Key performance indices, including peak overshoot, rise time, steady-state error, and settling time, were analyzed to quantify the system's ability to maintain stability during frequency changes. The results show that the proposed arrangement or model successfully returns the system to its nominal state (i.e., Δf = 0) while exhibiting improved transient characteristics compared with the benchmark models reported in previous studies.[29,30]

Figure 7 illustrates the Simulink model of a single-area gas turbine-based LFC system incorporating governor droop characteristics. The model consists of the valve positioner, governor, fuel system, compressor discharge volume, gas turbine, and power system blocks, which collectively represent the dynamic behavior of the gas turbine generating unit. The governor senses Δfs and adjusts the valve position based on the droop characteristic, while the fuel system and compressor discharge volume model fuel flow and combustion dynamics before the gas turbine delivers mechanical power. A ΔPL was applied to the power system to emulate sudden changes in load demand. The resulting Δf was fed back to the governor through the droop characteristic, enabling automatic adjustment of generator output. This closed-loop configuration represents the primary frequency control mechanism, ensuring that

the generation-load imbalance is minimized and system frequency is maintained within acceptable limits following ΔPLs. **Figure 8** illustrates the response to a change in load demand through the corresponding step response. The Δf gradually diminishes and reaches its steady-state value within 18 s, indicating rapid damping of transient oscillations and superior dynamic performance compared with the reference models presented in previous studies.[29,30]

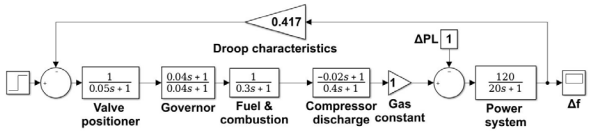


Figure 7. Block diagram of a single-area load frequency control system of a gas power generator

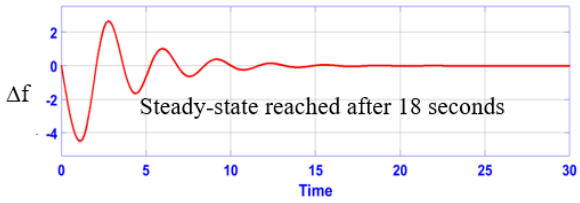


Figure 8. Results showing the step response of the system that reaches steady state (Δf = 0) after 18 s, once the transients subside.

Figure 9 depicts the model structure of the hydropower generator. **Figure 10** illustrates the system's corresponding step response following the ΔPL. The Δf gradually attenuates and reaches its steady-state value within 16 s. This behavior indicates relatively faster damping of transient oscillations and enhanced dynamic stability compared with the previously investigated models.

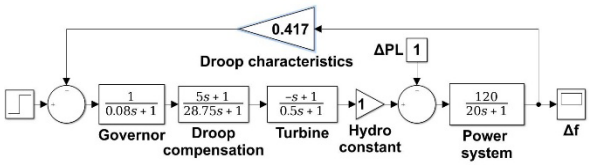


Figure 9. Block diagram of a single-area load frequency control system incorporating a hydro power generator

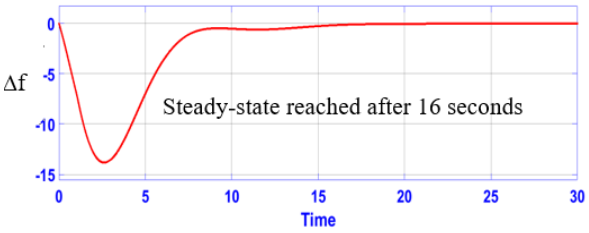


Figure 10. Simulation results reveal that the system attains steady-state operation with zero frequency error (Δf = 0) after nearly 16 s, once the transient oscillations have diminished

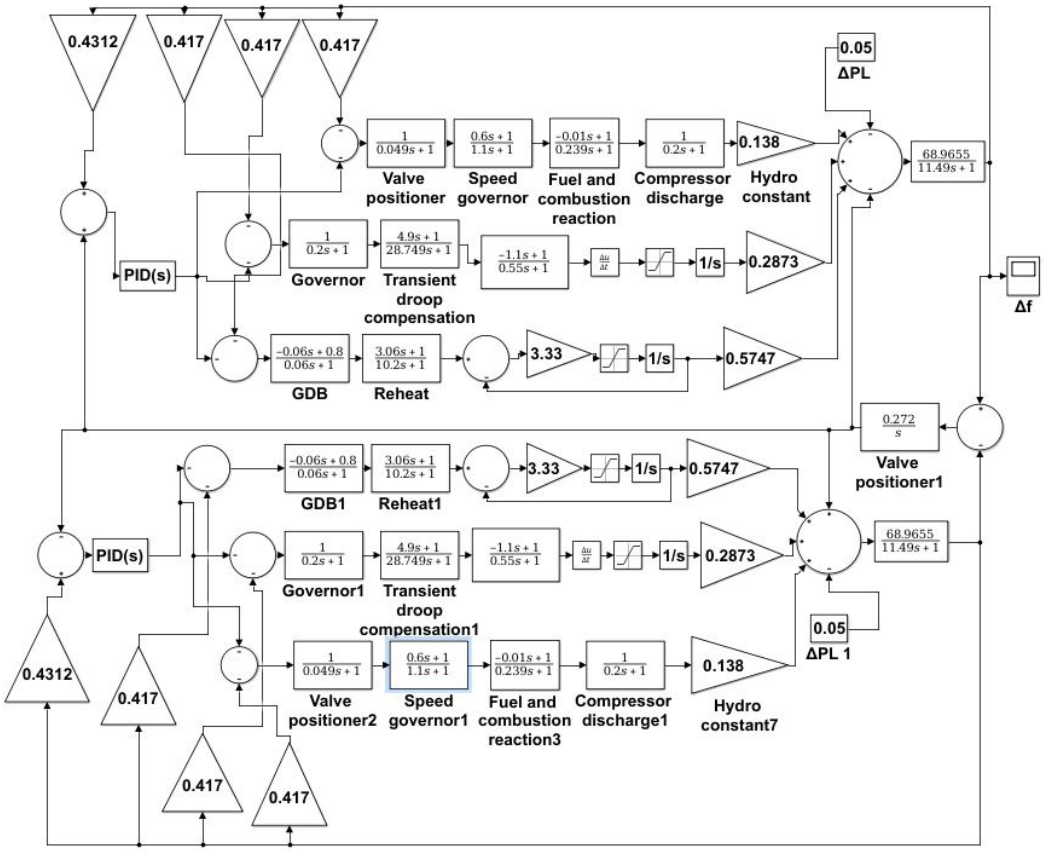


Figure 11. Simulink implementation of the two-area multi-source interconnected power system model used for load frequency control analysis

Figure 11 illustrates the model structure of a dynamic formulation of an interconnected 2-area power network with multiple energy sources. **Figure 12** illustrates the system's response to a step input following the ΔPL. The Δf diminishes and reaches its steady-state value after about 30 s, showing attenuated oscillations and successful restoration of system frequency under minimal operating conditions.

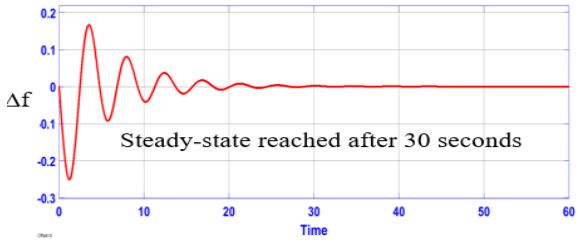


Figure 12. The step response of the model shows that the zero-frequency deviation (Δf = 0) is reached after nearly 30 s, once the transient oscillations have diminished

4. Estimation/Characterization of limit cycles

The estimation/characterization of LCs investigates the dynamics of the LFC system under governor backlash nonlinearity. Because of the governor's underlying nonlinear behavior, LC oscillations may arise even under stable operating conditions, adversely affecting system performance and frequency regulation. The turbine–generator–governor framework, incorporating governor backlash effects, was simulated to assess nonlinear oscillations. Δf responses were recorded over time, and the resulting oscillatory patterns were analyzed for magnitude and periodicity to identify LCs and their impact on system performance.

To assess LCs, each model was investigated under autonomous operation with governor deadband/backlash nonlinearity included in the LFC loop. This nonlinearity generates oscillatory behavior in the system output, facilitating detection and characterization of LCs for each model.

The structure of the proposed model is presented in **Figure 13**, where governor nonlinearity in the form of backlash was included to reflect practical implementation conditions. This arrangement permits the investigation of the system's nonlinear dynamic output. **Figure 14** presents the equivalent simulation results, which demonstrate the occurrence of an LC in the system output. The observed oscillations clearly indicate an LC frequency of 2.0 rad/s, confirming nonlinear oscillations generated by governor backlash nonlinearity.

The structure of the proposed model is presented in **Figure 15**, where governor nonlinearity in the form of backlash was included to reflect practical implementation conditions.[29] This arrangement facilitates the investigation of the nonlinear dynamic characteristics for the corresponding system. **Figure 16** illustrates the equivalent Simulink response, revealing the occurrence of an LC. The system outputs sustained oscillations at 1.50 rad/s, confirming the nonlinear effects introduced by governor backlash and demonstrating their impact on the system's overall performance and stability.

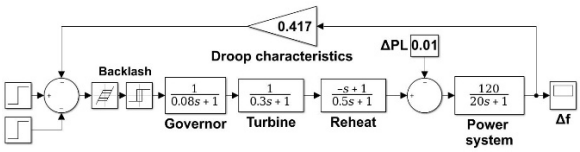


Figure 13. Block diagram of a single-area load frequency control system shown in **Figure 3**'s thermal generator with reheat system

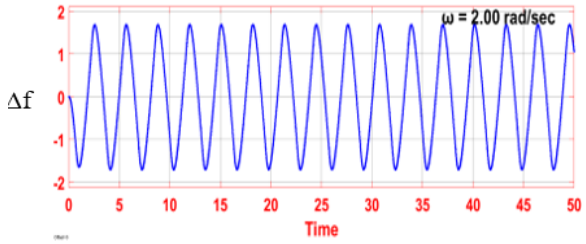


Figure 14. Results show the limit cycle of the model shown in **Figure 13** at a frequency of 2.0 rad/s

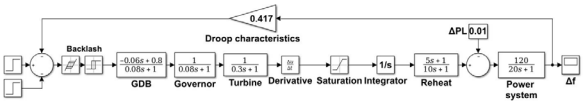


Figure 15. Block diagram of the model shown in **Figure 5**'s thermal generator with generation rate constraint and governor deadband nonlinearity

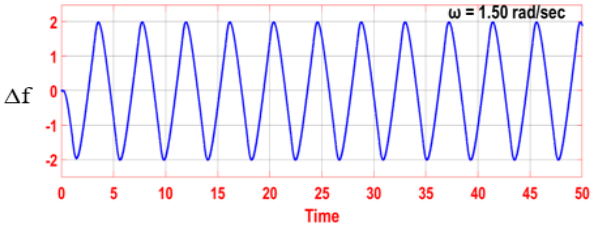


Figure 16. Results show the limit cycle excitation of the model shown in **Figure 15** at a frequency of 1.50 rad/s

Figure 17 depicts the model structure of the proposed sample, where nonlinearity (backlash) was incorporated into the governor to emulate its practical implementation. **Figure 18** shows the equivalent Simulink outputs, demonstrating the occurrence of an LC. The oscillations in Δf occurred at ω = 1.69 rad/s, confirming nonlinear dynamics induced by governor backlash in the proposed structure.

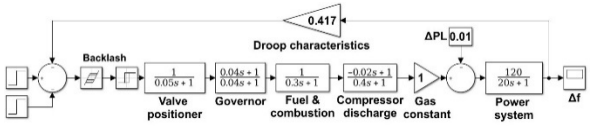


Figure 17. Block diagram of the model shown in **Figure 7** of the gas power generator with deadband

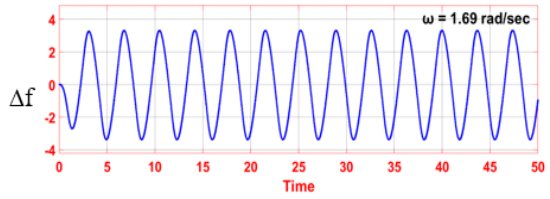


Figure 18. Results show the exposition of the limit cycle of the model shown in **Figure 17** with ω = 1.69 rad/s

Figure 19 illustrates the model structure of the hydropower system, in which the governor has inherent backlash characteristics. **Figure 20** illustrates the simulation output, exhibiting the LC, with a frequency of 0.5 rad/s.

Figure 21 depicts the model structure of the dynamic model of the two-area multi-source interconnected power system. **Figure 22** illustrates the equivalent Simulink output, revealing the occurrence of LC. The observed oscillations occurred at ω = 2.03 rad/s, confirming nonlinear oscillations generated by governor backlash and demonstrating its influence on the stability of the interconnected power system.

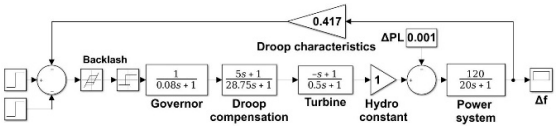


Figure 19. Block diagram of a hydro power generator with a deadband

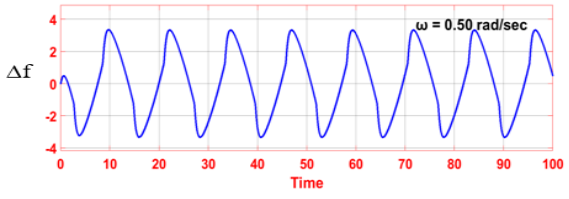


Figure 20. Results show the limit cycle with a frequency of 0.50 rad/s in the hydro power generator model

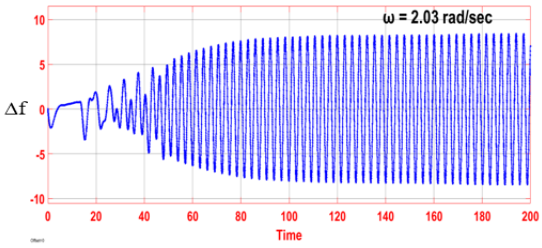


Figure 22. Results show the limit cycle behavior of the model shown in **Figure 21** at a frequency of 2.03 rad/s

5. Signal stabilization/output regulation using deterministic and Gaussian signals

The models investigated in Section 4 demonstrate self-sustained oscillatory behavior, commonly referred to as LCs. These oscillations can be mitigated or eliminated by adding high-frequency dither signals. Frequencies are generally selected to be at least 10 times higher than

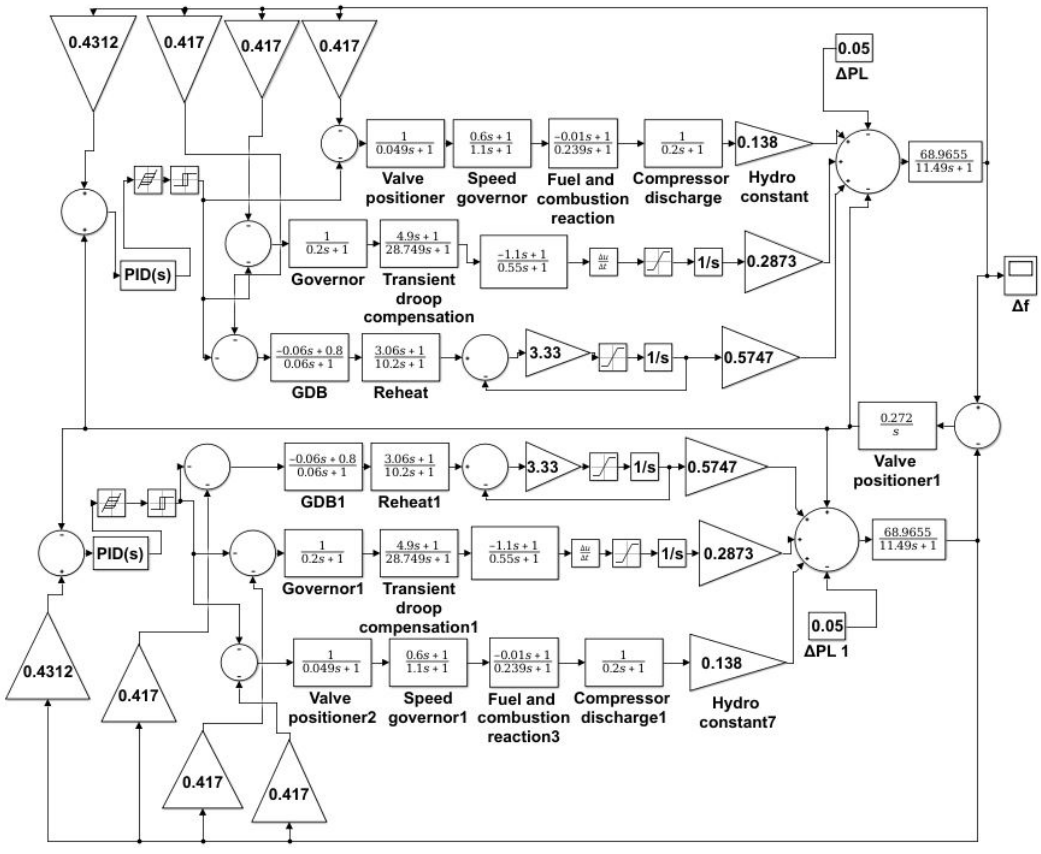


Figure 21. Simulink arrangement of the dynamic model shown in **Figure 11**

the LC frequencies determined for each model.[22,57] These signals effectively quench LCs and mitigate undesirable oscillations without significantly degrading the overall system response.[19–22]

Figure 23 depicts the model structure presented in Khan *et al.*[29], configured for oscillation mitigation using a deterministic dither signal (5 sin ωt, ω = 20 rad/s). **Figure 24** illustrates the model structure stabilized using a Gaussian random process with a mean of 100 and a variance of 0.5. The signal shows small random deviations due to the system's stochastic nature, which interfere with and mitigate LC-linked oscillations. **Figure 25** shows that the model response aligns with the input deterministic signal, while **Figure 26** confirms LC quenching and reestablished stability in the LFC model[29], with Δf settling at 0.

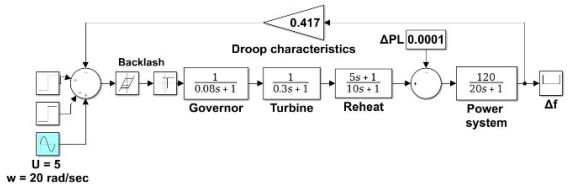


Figure 23. Simulink diagram showing signal stabilization of the proposed model in **Figure 3** using a deterministic signal-stabilized thermal generator with a reheat system

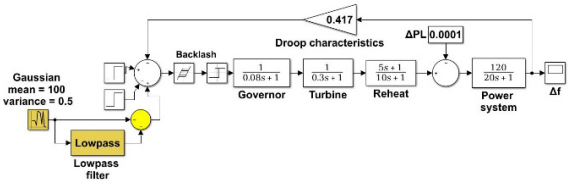


Figure 24. Simulink diagram of the signal-stabilized proposed model of **Figure 3** using a Gaussian signal

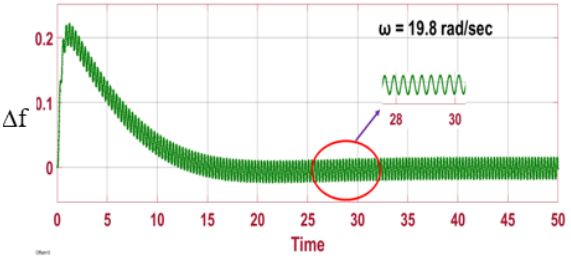


Figure 25. Response exhibiting the signal stabilization of the model shown in **Figure 23** using a deterministic signal

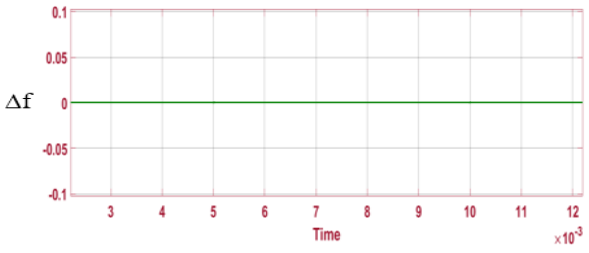


Figure 26. Response showing signal stabilization of the model shown in **Figure 24** using a Gaussian signal

Figure 27 illustrates the model structure presented in Khan *et al.*[29], configured for stabilization using a deterministic dither signal (5 sin ωt, ω = 15 rad/s). The selected excitation frequency was 10 times the limit cycle frequency of 1.5 rad/s, enabling effective mitigation of backlash-induced oscillations. **Figure 28** depicts the system under Gaussian random excitation with a mean amplitude of 100 and a variance of 0.5. **Figure 29** depicts the model output in sync with the applied deterministic excitation. **Figure 30** depicts the stabilized response obtained using the Gaussian excitation. The results confirm successful elimination of oscillatory behavior and restoration of steady-state operation with a Δf.

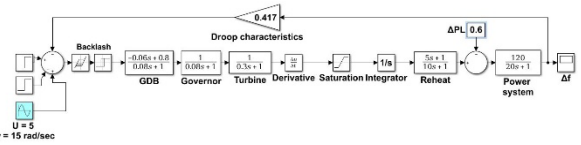


Figure 27. Simulink diagram showing the stabilized thermal generator with generation rate constraint (GRC) and governor deadband (GDB) nonlinearities using a deterministic signal

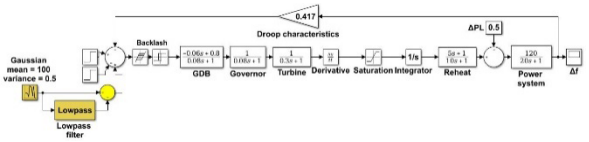


Figure 28. Simulink diagram showing the signal stabilization using a random Gaussian signal

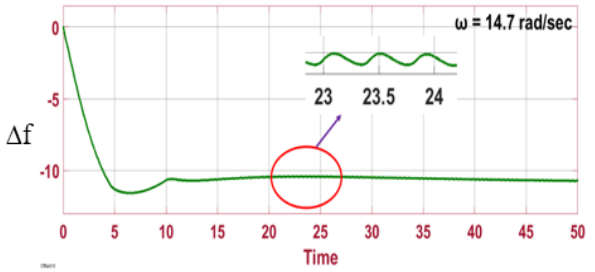


Figure 29. System shown in **Figure 5** synchronized to the signal stabilization model shown in **Figure 27**

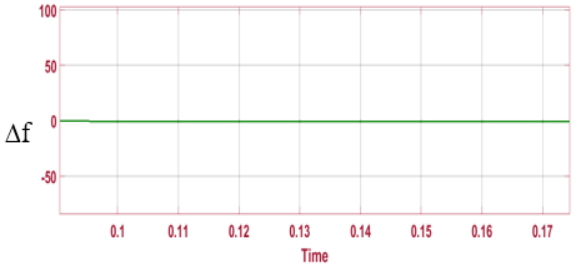


Figure 30. The stabilized system response of the model depicted in **Figure 28** when subjected to a Gaussian input signal

Figure 31 illustrates the model structure presented in Khan *et al.*[29], designed to achieve stabilization through

a deterministic dither signal (5 sin ωt, ω = 17 rad/s). The selected excitation frequency was 10 times the LC frequency of 1.67 rad/s, enabling effective mitigation of governor-induced oscillations. **Figure 32** depicts the equivalent model stabilized using a Gaussian random process with a mean amplitude of 100 and variance = 0.5. As shown in **Figure 33**, the system output tracks and remains synchronized with the deterministic excitation, while **Figure 34** shows the stabilized output corresponding to the Gaussian input signal. The response confirms the attenuation of oscillatory dynamics and the attainment of steady-state operation with Δf=0.

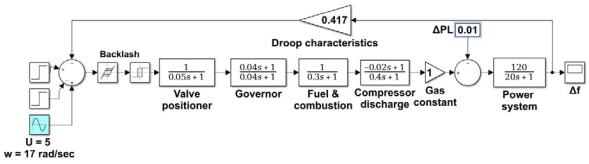


Figure 31. Simulink implementation of the nonlinear governor-controlled power system, including deadband/backlash effects and associated turbine–generator dynamics

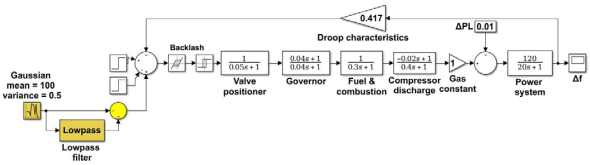


Figure 32. Simulink configuration illustrating system stabilization under Gaussian noise excitation having a mean of 100 and a variance of 0.5



Figure 33. Results showing the response characteristics of the stabilization framework presented in Khan *et al.*[29] under a deterministic input signal

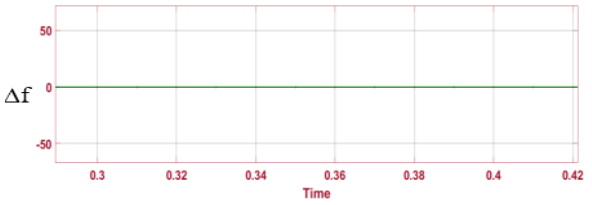


Figure 34. Results depicting the response characteristics of the controlled system in the presence of a Gaussian input signal.

Figure 35 illustrates the model structure presented in Khan *et al.*[29], designed to stabilize the system through a deterministic dither signal (5 sin ωt, ω=5 rad/s). The selected excitation frequency was 10 times the LC frequency of 0.5 rad/s, ensuring effective mitigation of governor-induced oscillations. **Figure 36** depicts the equivalent model stabilized using a Gaussian random process with a mean amplitude of 100 and variance = 0.5. **Figure 37** illustrates the system output in sync with the applied deterministic excitation, while the stabilized output corresponding to the Gaussian input signal is shown in **Figure 38**. The response confirms attenuation of oscillatory dynamics and attainment of steady-state operation with Δf = 0.

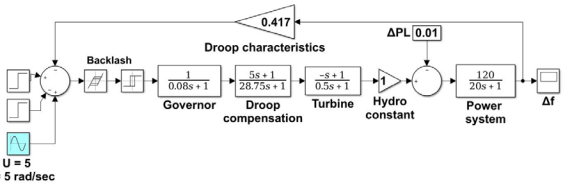


Figure 35. Simulink-based model used to analyze the stabilization characteristics of the system under a sinusoidal deterministic excitation with ω = 5 rad/s

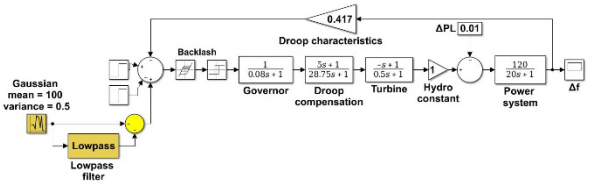


Figure 36. Simulink representation of the proposed system used for analyzing stability behavior under a Gaussian random process characterized by a mean of 100 and a variance of 0.5

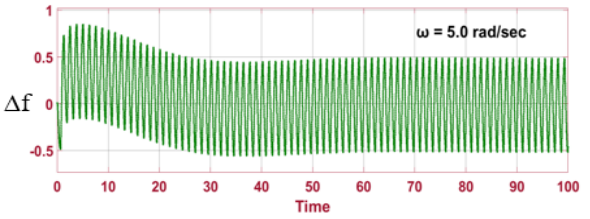


Figure 37. System response illustrating signal stabilization under deterministic excitation, with synchronization achieved at an angular frequency of 5 rad/s

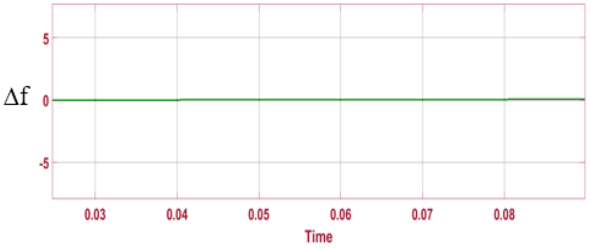


Figure 38. Response showing the signal stabilization using a Gaussian signal with no oscillations (mean of 100 and variance of 0.5

Figure 39 illustrates the model structure presented in Tavakoli *et al.*[30], designed to achieve stabilization through a deterministic dither signal (5 sin ωt, ω=20 rad/s). The excitation frequency was 10 times the LC frequency of

2.0 rad/s, enabling effective mitigation of the oscillations induced by the governor. **Figure 40** depicts the equivalent model stabilized using a Gaussian random process characterized by a mean amplitude of 100 and variance = 0.5. As depicted in **Figure 41**, the system output successfully tracks and remains synchronized with the deterministic excitation. The stabilized output corresponding to the Gaussian input signal is shown in **Figure 42**. The response confirms the attenuation of oscillatory dynamics and the attainment of steady-state operation with $\Delta f = 0$.

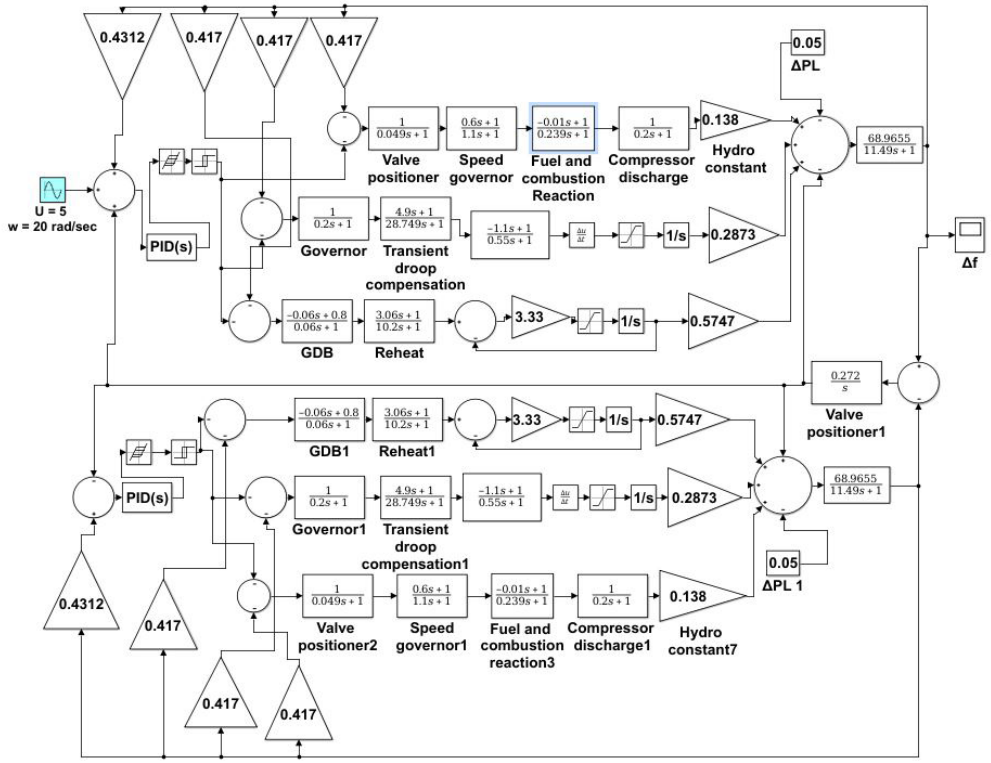


Figure 39. Simulink model of the interconnected power system used to investigate frequency stabilization and dynamic performance under external excitation signals using a deterministic signal of 5 sin ωt, where ω = 20 rad/s

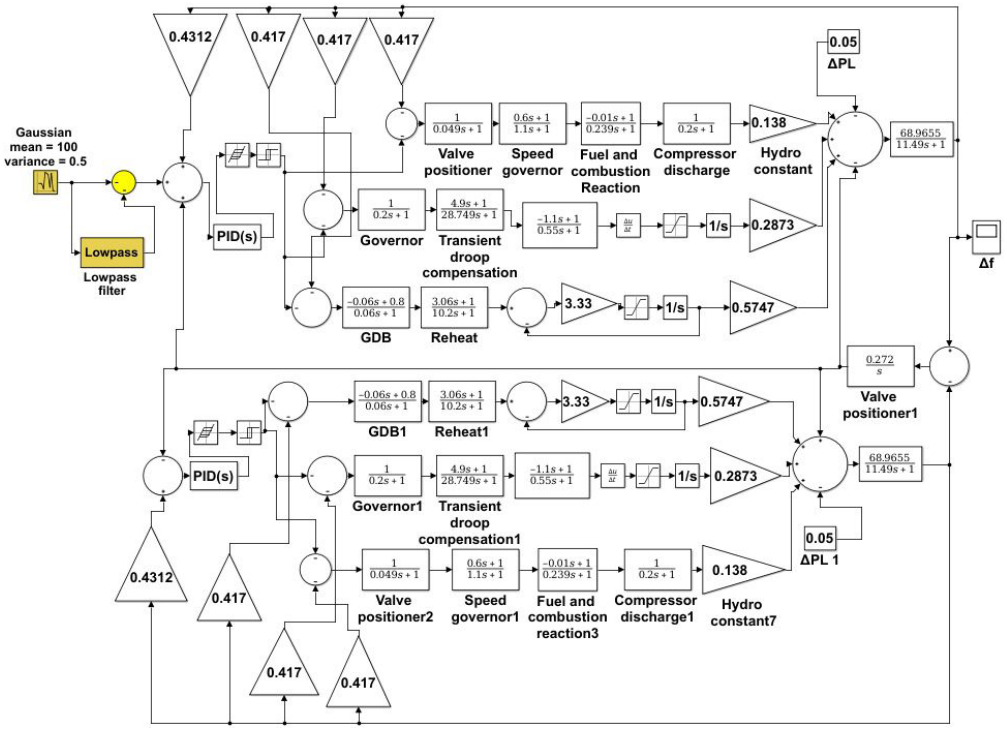


Figure 40. Simulink model of the interconnected power system used to investigate frequency stabilization and dynamic performance under external excitation signals using a random Gaussian signal with a mean of 100 and variance of 0.5

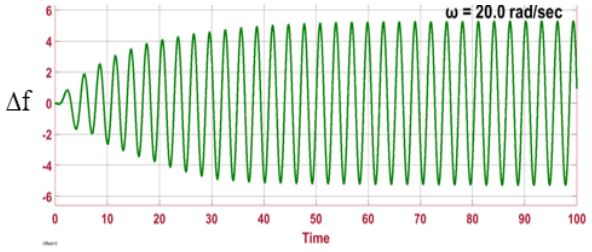


Figure 41. Frequency deviation response exhibiting sustained oscillations under autonomous operating conditions at an angular frequency of ω = 20 rad/s

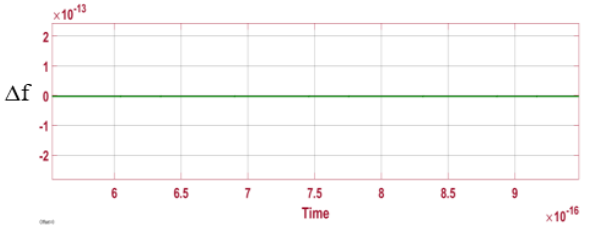


Figure 42. Steady-state frequency deviation response showing convergence to Δf = 0, indicating stable system operation (Gaussian excitation)

6. Signal stabilization using a digital deadbeat controller

The digital deadbeat controller (DDC) was incorporated into every model, as discussed in previous sections, to achieve fast and accurate frequency stabilization over the course of the LFC scheme. The main aim is to eliminate steady-state error in the system response, attenuate oscillations, and provide a response free from transients and ripple, even in the presence of nonlinearities (backlash and deadband). **Figure 43** presents the Simulink diagram of the DDC, illustrating its basic architecture and operation within the overall control system.

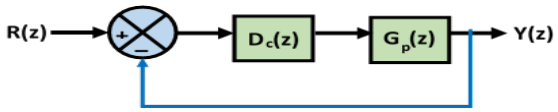


Figure 43. Discrete-time closed-loop control system with unity feedback, showing the controller D(z), plant $G_p(z)$, reference input R(z), and output response Y(z)

The closed-loop transfer function in **Figure 43** was calculated by comparing the reference input R(z) (=U sin $\omega_f t$) with the output Y(z) to produce the error. This error was passed through the controller D(z), which generates the control action. The plant $G_p(z)$ then processes this signal to produce the output Y(z). The output was fed back directly (unity feedback) and subtracted from the reference to continuously reduce the error (**Equation 4**):[59]

$$\text{CLTF} = \frac{Y(z)}{R(z)} = \frac{1}{Z^n} \tag{4}$$

where n is the relative degree of the system, i.e., the number of poles minus the number of zeros.

The corresponding Z-transform is shown in **Equation 5:**

$$Z[U \sin \omega_f t] = \frac{U\, z \sin \omega_f T}{z^2 - 2z \cos \omega_f T + 1} \tag{5}$$

where $n = 1$.

Hence,

$$\frac{1}{Z^n} = \frac{1}{Z^1} = z^{-1} \tag{6}$$

Within the Simulink environment, a unit-delay block represented by z^{-1} was incorporated and applied to the stabilized signal, as shown in **Figures 44**, **46**, **48**, **50**, and **52**. The response profiles in **Figures 45**, **47**, **49**, **51**, and **53** validate the effectiveness of the proposed DDC. The controller rapidly damps transient dynamics, prevents sustained oscillations, and maintains a stable steady-state response across a range of operating conditions.

The Simulink representation of the reference model adopted from Khan *et al.*[29] is shown in **Figure 44** with a DDC and a deterministic excitation. **Figure 45** illustrates the equivalent system output, free from transients and ripples, achieving steady-state error = 0, and restoring the nominal frequency in the least time, thereby demonstrating the superior dynamic performance of the proposed control strategy.

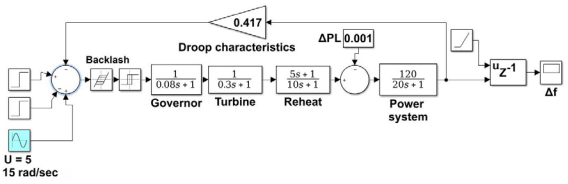


Figure 44. Block diagram of the digital deadbeat controller applied to the thermal generator with reheat system shown in **Figure 3** in the presence of a deterministic signal (forced signal stabilization)

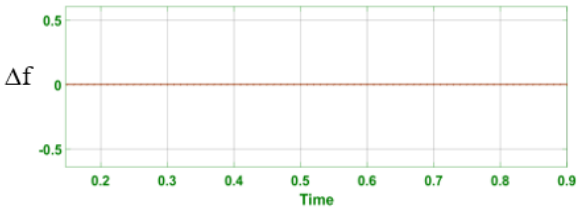


Figure 45. Simulation result shown in **Figure 3** using a digital deadbeat controller in the presence of a deterministic signal (forced signal stabilization)

Figure 46 illustrates the model structure presented in Khan *et al.*[29], incorporating a DDC using deterministic excitation. **Figure 47** illustrates the equivalent frequency response, which is free from transient oscillations and ripples, exhibits zero steady-state error, and reaches the desired operating point within the minimum achievable settling time, demonstrating near-optimal regulation.

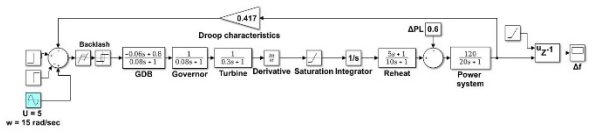


Figure 46. Simulink diagram of signal stabilization of the model shown in **Figure 5** with the application of a digital deadbeat controller in the presence of a deterministic signal (signal stabilization)

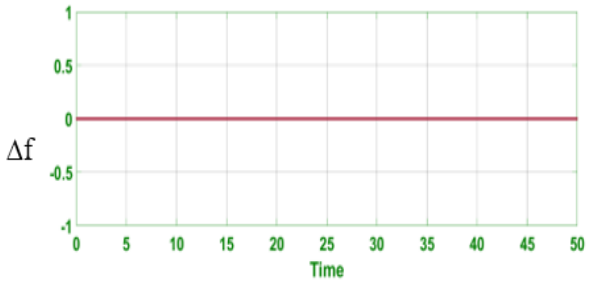


Figure 47. Simulation result shown in **Figure 5** using a digital deadbeat controller in the presence of a deterministic signal (for signal stabilization)

The model configuration shown in **Figure 48** incorporates a DDC and a deterministic excitation signal to stabilize the system. **Figure 49** illustrates the equivalent system output, which is free from transient oscillations and ripples, exhibits zero steady-state error, and attains the desired operating condition within the minimum achievable settling time, demonstrating virtually the fastest frequency regulation.

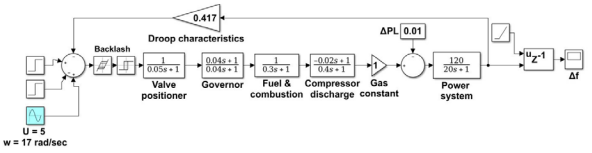


Figure 48. Simulink diagram of the model shown in **Figure 7** using a digital deadbeat controller with a deterministic excitation signal

The model configuration shown in **Figure 50** incorporates a DDC and a deterministic excitation signal to stabilize the system. **Figure 51** illustrates the equivalent system output, which is free from transient oscillations and ripples, exhibits zero steady-state error, and attains the desired operating condition within the minimum achievable settling time, demonstrating virtually the fastest frequency regulation. **Figures 52** and **53** show the model incorporating DDC and its corresponding output, respectively.

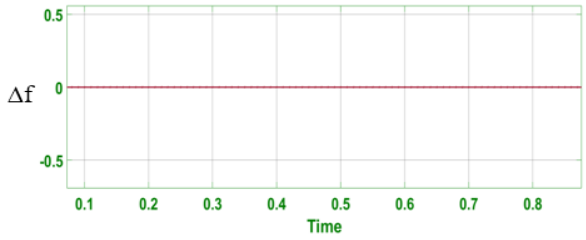


Figure 49. Stabilization performance of the digital deadbeat controller-controlled system in the presence of a deterministic forcing signal

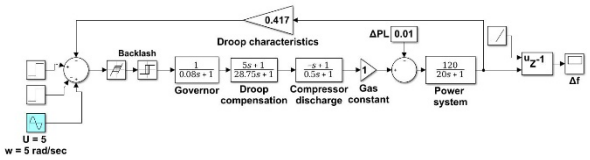


Figure 50. Simulink diagram of the model shown in **Figure 9** with the digital deadbeat controller and deterministic signal (for signal stabilization)

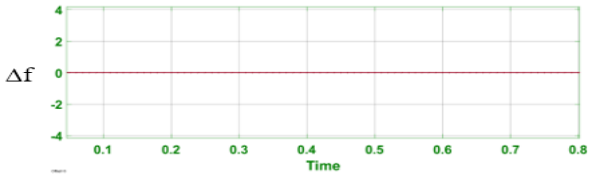


Figure 51. Simulation result shown in **Figure 9** with the application of the digital deadbeat controller in the presence of deterministic / forcing signal (for signal stabilization)

Table 1 summarizes the LFC performance comparison among the models reported in previous studies[29,30], the proposed system model, and the corresponding control **Table 1**. Performance comparison of conventional and advanced controllers in load frequency control systems

Table 1. Performance comparison of conventional and advanced controllers in load frequency control systems

Models	**Performance in load frequency control**				
	Step response	**Estimation of limit cycles (LCs)**	**Signal stabilization by deterministic signal**	**Signal stabilization by Gaussian signal**	**Application of digital deadbeat controller**
Thermal generator with reheat system in **Figure 3**[29]	Steady state Δf = 0; transient continuous up to 20 s in **Figure 4**	LC observed: ω = 2.0 rad/s in **Figure 14**	Synchronized to ω = 19.8 rad/s in **Figure 25**	Stabilized fully at steady state; time taken in the least time s at Δf = 0 in **Figure 26**	Steady value Δf = 0; time to reach steady state in the least time in **Figure 45**

(*Cont'd...*)

Table 1. (*Continued*)

Models	Performance in load frequency control				
	Step response	**Estimation of limit cycles (LCs)**	**Signal stabilization by deterministic signal**	**Signal stabilization by Gaussian signal**	**Application of digital deadbeat controller**
Thermal generator with GRC & GDB nonlinearities (Backlash) in **Figure 5**[29]	Steady state Δf = 0; transient continuous up to 20 s in **Figure 6**	LC observed: ω = 1.5 rad/s in **Figure 16**	Synchronized to ω = 14.7 rad/s in **Figure 29**	Stabilized fully at steady state; time taken in the least time s at Δf = 0 in **Figure 30**	Steady state Δf = 0; time to reach steady state in the least time in **Figure 47**
Gas power generator in **Figure 7**[29]	Steady state Δf = 0; transient continuous up to 18 s in **Figure 8**	LC observed: ω = 1.69 rad/s in Figure 18	Synchronized to ω = 16.7 rad/s in **Figure 33**	Stabilized fully at steady state; time taken in the least time s at Δf = 0 in **Figure 34**	Steady state Δf = 0; time to reach steady state in the least time in **Figure 49**
Hydro power generator in **Figure 9**[29]	Steady state Δf = 0; transient continuous up to 16 s in **Figure 10**	LC observed: ω = 0.5 rad/s in **Figure 20**	Synchronized to ω = 5.0 rad/s in **Figure 37**	Stabilized fully at steady state; time taken in the least time s at Δf = 0 in **Figure 38**	Steady state Δf = 0; time to reach steady state in the least time in **Figure 51**
Dynamic model of two-area multi-source interconnected power system in **Figure 11**[30]	Steady state Δf = 0; transient continuous up to 30 s in **Figure 12**	LC observed: ω = 2.03 rad/s in **Figure 22**	Synchronized to ω = 20 rad/s in **Figure 41**	Stabilized fully at steady state; time taken in the least time s at Δf = 0 in **Figure 42**	Steady state Δf = 0; time to reach steady state in the least time in **Figure 53**

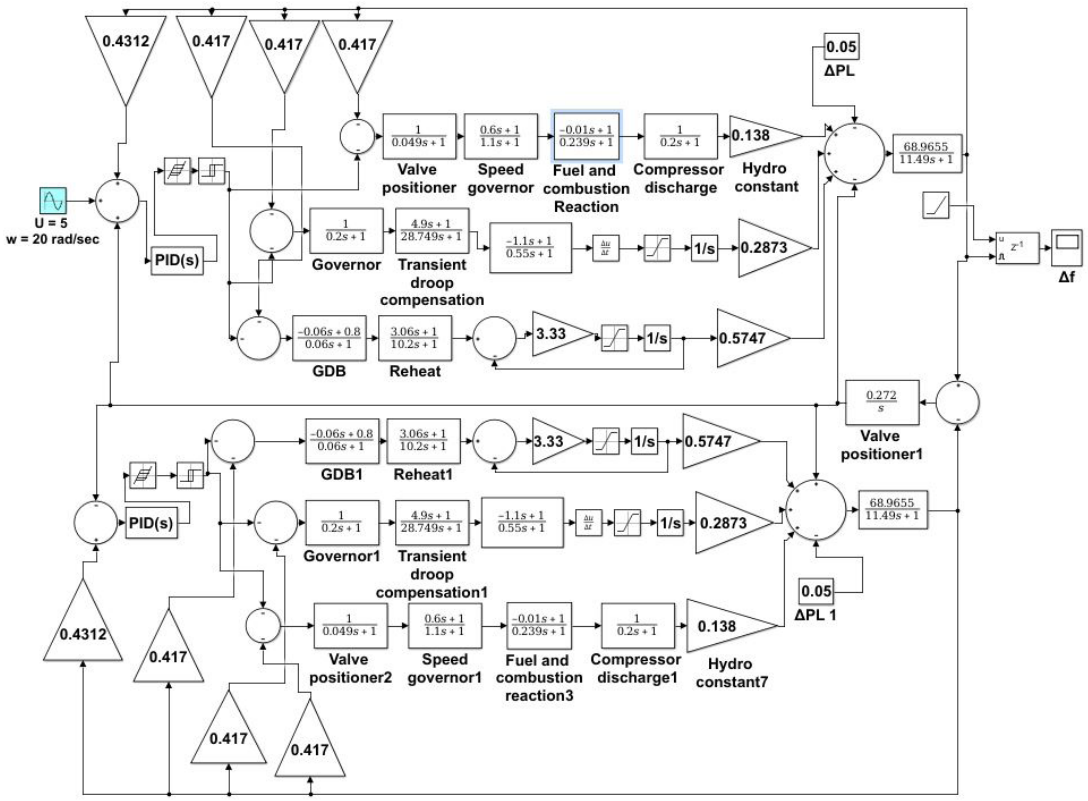


Figure 52. Simulink diagram of the model shown in **Figure 11** with the application of a digital deadbeat controller in the presence of a deterministic forcing signal (for signal stabilization)

strategies, including robust PID, proportional-integral and proportional-derivative, and the proposed DDC. The parameters used in all the figures are shown in **Table A1**.

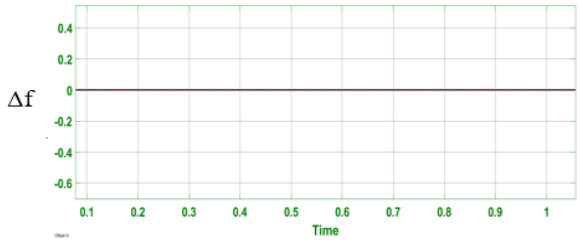


Figure 53. Simulation result of the model shown in **Figure 11** with the application of a digital deadbeat controller in the presence of a deterministic/forcing signal (for signal stabilization)

7. Conclusion

A major technical contribution of the present work is integrating signal stabilization via high-frequency dither signals (deterministic/random [Gaussian]) with a DDC to mitigate self-sustained nonlinear oscillations (LC) arising from governor backlash in the least time.

The proposed framework offers a practical and scalable solution for enhancing frequency stability and reliability in future intelligent interconnected power systems with high penetration of renewable energy sources, distributed generation, energy storage, and electric vehicles. These findings, and the rapid response in particular, establish a strong foundation for future research on real-time implementation, adaptive and artificial intelligence-driven controllers, and next-generation resilient power system operation.

The present work considers the most vital models such as: (i) a thermal generator with reheat system (**Figure 3**)[29], (ii) a thermal generator with GRC and GDB nonlinearities (Backlash) (**Figure 5**)[29], (iii) a gas power generator (**Figure 7**)[29], (iv) a hydropower generator (**Figure 9**)[29], and (v) a dynamic model of a two-area multi-source interconnected power system (**Figure 11**).[30]

The LFC simulation study faces major challenges from renewable energy integration, low system inertia, complex load variations, and stochastic load demands.

In addition to a high-frequency deterministic dither signal, a random (Gaussian) signal was used to eliminate or mitigate LC oscillations, providing robust uncertainty handling when additional DDC may not be required.

Signal stabilization, implemented using deterministic and Gaussian excitation signals, effectively quenches or mitigates LC oscillations and significantly enhances system stability. Comparative analyses show that the DDC consistently provides superior dynamic performance by achieving rapid frequency restoration with negligible transient oscillations, ripple-free operation, and zero steady-state error in the least time. Notably, Gaussian signal stabilization alone can also produce a fast, transient-free, ripple-free response while effectively mitigating oscillations, although a small steady-state Δf may persist. Combining signal stabilization and DDC eliminates this residual error, yielding the best overall dynamic performance among the investigated approaches.

Acknowledgments

The authors thank C.V. Raman Global University, Bhubaneswar, Odisha, India, for providing computer facilities for preparing this manuscript.

Funding

None.

Conflict of interest

The authors declare they have no competing interests.

Author contributions

Conceptualization: Kartik Chandra Patra
Formal analysis: Asutosh Patnaik
Investigation: Kartik Chandra Patra
Methodology: Kartik Chandra Patra
Writing–original draft: Kartik Chandra Patra, Asutosh Patnaik
Writing–review & editing: Kartik Chandra Patra, Asutosh Patnaik

Availability of data

The datasets generated during and/or analysed during the current study are available from the corresponding author on reasonable request.

AI tools statement

AI tool ChatGPT was used in the preparation of this manuscript.

References

1. Jain D, Saxena D. Comprehensive review on control schemes and stability investigation of hybrid AC-DC microgrid. *Electr Power Syst Res.* 2023;218:109182.

   https://doi.org/ 10.1016/j.epsr.2023.109182

2. Yang S, Fan X, Zhao Y, Hao Z, Zhang B, Hojo M. A novel method for transient stability margin evaluation of the post-disturbance power system. In: Proceeding of the 15th International Conference on Developments in Power System Protection (DPSP 2020). London: Institution of Engineering and Technology; 2020:5.

   https://doi.org/ 10.1049/cp.2020.0048

3. Dong X, Hao X, Chen Q, Wang C, Wang M. A Distributed power transfer limit calculation method for Multi-Area interconnection power networks. *IEEE Trans Power Syst.* 2021;36(5):4723-4732.

   https://doi.org/ 10.1109/tpwrs.2021.3062374

4. Tungadio DH, Sun Y. Load frequency controllers considering renewable energy integration in power system. *Energy Rep.* 2019;5:436-453.

   https://doi.org/ 10.1016/j.egyr.2019.04.003

5. Ashfaq T, Mumtaz S, Ahmad S, Ullah B, Albogamy FR. Automatic Generation control in Renewables-Integrated

Multi-Area Power Systems: A Comparative control analysis. *Sustainability*. 2024;16(13):5735.

https://doi.org/ 10.3390/su16135735

6. Gulzar MM, Iqbal M, Shahzad S, Muqeet HA, Shahzad M, Hussain MM. Load Frequency Control (LFC) Strategies in Renewable Energy-Based Hybrid Power Systems: A review. *Energies*. 2022;15(10):3488.

https://doi.org/ 10.3390/en15103488

7. Kothari. *Modern Power System Analysis*. New Delhi: Tata McGraw-Hill Education; 2011.

8. Mi Y, Fu Y, Wang C, Wang P. Decentralized sliding Mode load frequency control for Multi-Area power systems. *IEEE Trans Power Syst.* 2013;28(4):4301-4309.

https://doi.org/ 10.1109/tpwrs.2013.2277131

9. Aldeen M, Marsh JF. Decentralised proportional-plus-integral design method for interconnected power systems. *IEE Proc C Gener Transm Distrib UK*. 1991;138(4):263.

https://doi.org/ 10.1049/ip-c.1991.0033

10. Khodabakhshian A, Hooshmand R. A new PID controller design for automatic generation control of hydro power systems. *Int J Electr Power Energy Syst.* 2009;32(5):375-382.

https://doi.org/ 10.1016/j.ijepes.2009.11.006

11. Alrifai MT, Hassan MF, Zribi M. Decentralized load frequency controller for a multi-area interconnected power system. *Int J Electr Power Energy Syst.* 2010;33(2):198-209.

https://doi.org/ 10.1016/j.ijepes.2010.08.015

12. Tan W. Tuning of PID load frequency controller for power systems. *Energy Convers Manag.* 2009;50(6):1465-1472.

https://doi.org/ 10.1016/j.enconman.2009.02.024

13. Juang CF, Lu CF. Power system load frequency control by evolutionary fuzzy PI controller. In: 2004 IEEE International Conference on Fuzzy Systems (IEEE Cat. No.04CH37542). Vol 2. Piscataway, NJ, USA: IEEE; 2004:715-719.

https://doi.org/ 10.1109/fuzzy.2004.1375486

14. Kocaarsian I, Cam E. Fuzzy logic controller in interconnected electrical power systems for load-frequency control, *Int J Electri Power Energy Syst*. 2005;27(8):542-549.

https://doi.org/ 10.1016/j.ijepes.2005.06.003

15. Mathur HD, Manjunath HV. Extended Fuzzy Logic Based Integral Controller for Three Area Power System with Generation Rate Constraint. In: 2006 IEEE International Conference on Industrial Technology. Piscataway, NJ, USA: IEEE; 2006:917-921.

https://doi.org/ 10.1109/icit.2006.372279

16. Moon YH, Ryu HS, Lee JG, Song KB, Shin MC. Extended integral control for load frequency control with the consideration of generation-rate constraints. *Int J Electr Power Amp Energy Syst.* 2002;24(4):263-269.

https://doi.org/ 10.1016/s0142-0615(01)00036-9

17. Tsay TS. Load–frequency control of interconnected power system with governor backlash nonlinearities. *Int J Electr Power Energy Syst.* 2011;33(9):1542-1549.

https://doi.org/ 10.1016/j.ijepes.2011.06.005

18. Chidambaram IA, Velusami S. Decentralized Biased Controllers for Load-Frequency Control of Interconnected Power Systems Considering Governor Dead Band Non-Linearity. In: 2005 Annual IEEE India Conference. Piscataway, NJ, USA: IEEE; 2005:521-525.

https://doi.org/ 10.1109/indcon.2005.1590225

19. Patra KC, Kar N, Patnaik A. Suppression limit cycles in 2x2 nonlinear systems with memory type nonlinearities. *Des Constr Maint.* 2024;4:169-185.

https://doi.org/ 10.37394/232022.2024.4.18

20. Wang C, Yang M, Zheng W, Hu K, Xu D. Analysis and suppression of limit cycle oscillation for transmission system with backlash nonlinearity. *IEEE Trans Ind Electron.* 2017;64(12):9261-9270.

https://doi.org/ 10.1109/tie.2017.2711564

21. Patra KC, Patnaik A. Investigation of Limit Cycles and Signal Stabilization by Deterministic and Gaussian Random Signals Based on Deadbeat Approach in 3×3 Nonlinear Systems with Memory Nonlinearities. *Int J Electr Eng Comput Sci.* 2025;7:159-188.

https://doi.org/ 10.37394/232027.2025.7.17

22. Oldenburger R, Nakada T. Signal stabilization of self-oscillating systems. *IRE Trans Autom Control.* 1959;4(3):37.

https://doi.org/ 10.1109/tac.1959.1104874

23. Magdy G, Shabib G, Elbaset AA, Mitani Y. Optimized coordinated control of LFC and SMES to enhance frequency stability of a real multi-source power system considering high renewable energy penetration. *Prot Control Mod Power Syst.* 2018;3(1).

https://doi.org/ 10.1186/s41601-018-0112-2

24. C S, Yammani C, Maheswarapu S. Load Frequency Control of Multi-microgrid System considering Renewable Energy Sources Using Grey Wolf Optimization. *Smart Sci*. 2019;7(3):198-217.

https://doi.org/ 10.1080/23080477.2019.1630057

25. Bevrani H, Golpîra H, Messina AR, Hatziargyriou N, Milano F, Ise T. Power system frequency control: An updated review of current solutions and new challenges. *Electr Power Syst Res*. 2021;194:107114.

https://doi.org/ 10.1016/j.epsr.2021.107114

26. Ahmed M, Magdy G, Khamies M, Kamel S. An efficient coordinated strategy for frequency stability in hybrid power systems with renewables considering interline power flow controller and redox flow battery. *J Energy Storage.* 2022;52:104835.

https://doi.org/ 10.1016/j.est.2022.104835

27. Cavdar B, Sahin E, Sesli E, Akyazi O, Nuroglu FM. Cascaded fractional order automatic generation control of a PV-reheat thermal power system under a comprehensive nonlinearity effect and cyber-attack. *Electr Eng.* 2023;105(6):4339-4360.

https://doi.org/ 10.1007/s00202-023-01943-y

28. Gulzar MM, Sibtain D, Alqahtani M, Alismail F, Khalid M. Load frequency control progress: A comprehensive review on recent development and challenges of modern power systems. *Energy Strategy Rev.* 2024;57:101604.

https://doi.org/ 10.1016/j.esr.2024.101604.

29. Khan IA, Mokhlis H, Mansor NN, Illias HA, Awalin LJ, Wang L. New trends and future directions in load frequency control

and flexible power system: A comprehensive review. *Alex Eng J.* 2023;71:263-308.

https://doi.org/ 10.1016/j.aej.2023.03.040

30. Tavakoli S, Zamani AA, Khajehoddin A. Efficient load frequency control in multi-source interconnected power systems using an innovative intelligent control framework. *Energy Rep.* 2024;11:2805-2817.

https://doi.org/ 10.1016/j.egyr.2024.02.037

31. Ali T, Malik SA, Hameed IA, Daraz A, Mujlid H, Azar AT. Load frequency control and automatic voltage regulation in a Multi-Area interconnected power system using Nature-Inspired Computation-Based control methodology. *Sustainability*. 2022;14(19):12162.

https://doi.org/ 10.3390/su141912162.

32. Loka R, Parimi AM, Srinivas STP, Kumar NM. Region of convergence by parameter sensitivity constrained genetic algorithm-based optimization for coordinated load frequency control in multi-source distributed hybrid power system. *Sustain Energy Technol Assess.* 2022;54:102887.

https://doi.org/ 10.1016/j.seta.2022.102887

33. Tripathi S, Singh VP, Kishor N, Pandey AS. Load frequency control of power system considering electric Vehicles' aggregator with communication delay. *Int J Electr Power Energy Syst.* 2022;145:108697.

https://doi.org/ 10.1016/j.ijepes.2022.108697

34. Alshammari B, Salah RB, Kahouli O, Kolsi L. Design of Fuzzy TS-PDC Controller for electrical power System via rules Reduction approach. *Symmetry*. 2020;12(12):2068.

https://doi.org/ 10.3390/sym12122068

35. Lawal MJ, Hussein SU, Saka B, Abubakar SU, Attah IS. Intelligent fuzzy-based automatic voltage regulator with hybrid optimization learning method. *Sci Afr.* 2023;19:e01573.

https://doi.org/ 10.1016/j.sciaf.2023.e01573

36. Suid MH, Ahmad MA. Optimal tuning of sigmoid PID controller using Nonlinear Sine Cosine Algorithm for the Automatic Voltage Regulator system. *ISA Trans.* 2022;128:265-286.

https://doi.org/ 10.1016/j.isatra.2021.11.037

37. Izci D, Ekinci S. An improved RUN optimizer based real PID plus second-order derivative controller design as a novel method to enhance transient response and robustness of an automatic voltage regulator. *e-Prime Adv Electr Eng Electron Energy.* 2022;2:100071.

https://doi.org/ 10.1016/j.prime.2022.100071

38. Altbawi SMA, Mokhtar ASB, Jumani TA, Khan I, Hamadneh NN, Khan A. Optimal design of Fractional order PID controller based Automatic voltage regulator system using gradient-based optimization algorithm. *J King Saud Univ Eng Sci.* 2024;36(1):32-44.

https://doi.org/ 10.1016/j.jksues.2021.07.009

39. Dakua BK, Sahoo B, Pati BB. Design of PIΛDM controller for a Fractional-Order Automatic Voltage regulator system. *IFAC-PapersOnLine*. 2022;55(1):649-654.

https://doi.org/ 10.1016/j.ifacol.2022.04.106

40. Li C, Feng C, Li J, Hu D, Zhu X. Comprehensive frequency regulation control strategy of thermal power generating unit and ESS considering flexible load simultaneously participating in AGC. *J Energy Storage.* 2023;58:106394.

https://doi.org/ 10.1016/j.est.2022.106394

41. Guo W, Wu F. Stability behavior of load adjustment and primary frequency control of pumped storage power plant with upstream and downstream surge tanks. *J Energy Storage.* 2023;60:106626.

https://doi.org/ 10.1016/j.est.2023.106626

42. Yu J, Liao S, Xu J. Frequency control strategy for coordinated energy storage system and flexible load in isolated power system. *Energy Rep.* 2022;8:966-979.

https://doi.org/ 10.1016/j.egyr.2022.02.133

43. Lian Z, Wen C, Guo F, Lin P, Wu Q. Decentralized secondary control for frequency restoration and power allocation in islanded AC microgrids. *Int J Electr Power Energy Syst.* 2023;148:108927.

https://doi.org/ 10.1016/j.ijepes.2022.108927

44. Gulzar MM, Iqbal A, Sibtain D, Khalid M. An innovative converterless solar PV control strategy for a grid connected hybrid PV/Wind/Fuel-Cell system coupled with battery energy storage. *IEEE Access*. 2023;11:23245-23259.

https://doi.org/ 10.1109/access.2023.3252891

45. Perninge M, Eriksson R. Optimal Tertiary Frequency Control in Power Systems with Market-Based Regulation. *IFAC-PapersOnLine*. 2017;50(1):4374-4381.

https://doi.org/ 10.1016/j.ifacol.2017.08.881

46. Carere F, Gatta FM, Geri A, Lauria S, Maccioni M, Nati L. Sardinia as a 100% renewable power system: A frequency stability study. *Sustain Energy Grids Netw.* 2022;32:100899.

https://doi.org/ 10.1016/j.segan.2022.100899

47. Liaqat MK, Safdar M, Ahmad H, Raza S, Riaz A. Line Impedance Modulator Design For Load Flow Control In a Hybrid Power System. In: 2020 IEEE 23rd International Multitopic Conference (INMIC). Piscataway, NJ, USA: IEEE; 2020:1-6.

https://doi.org/ 10.1109/inmic50486.2020.9318110

48. Ahmad G, Gulzar MM, Shakoor A, Habib S, Ahmad H. Speed Control of Wind Turbines System using Evolutionary Algorithm based Cascaded Controller. In: 2024 International Conference on Control, Automation and Diagnosis (ICCAD). Piscataway, NJ, USA: IEEE; 2024:1-6.

https://doi.org/ 10.1109/iccad60883.2024.10553876

49. Nasir A, Rasool I, Sibtain D, Kamran R. Adaptive Fractional Order PID Controller based MPPT for PV connected grid system under changing weather conditions. *J Electr Eng Technol.* 2021;16(5):2599-2610.

https://doi.org/ 10.1007/s42835-021-00782-w

50. Bahl V, Linninger AA. Hybrid simulation of continuous-discrete systems. In: *Computer Aided Chemical Engineering*. Elsevier; 2000:163-168.

https://doi.org/ 10.1016/s1570-7946(00)80029-2

51. Hiskens IA, Pai MA. Hybrid systems view of power system modelling. In: 2000 IEEE International Symposium on Circuits and Systems. Emerging Technologies for the 21st Century. Proceedings (IEEE Cat No.00CH36353). Vol 2. Presses Polytech. Univ. Romandes; 2000:228-231.

https://doi.org/ 10.1109/iscas.2000.856300

52. Hayat A, Sibtain D, Murtaza AF, Shahzad S, Jajja MS, Kilic H. Design and analysis of input capacitor in DC–DC boost converter for Photovoltaic-Based Systems. *Sustainability*. 2023;15(7):6321.

https://doi.org/ 10.3390/su15076321

53. Tripathy SC, Bhatti TS, Jha CS, Malik OP, Hope GS. Sampled Data Automatic Generation Control Analysis with Reheat Steam Turbines and Governor Dead-Band Effects. *IEEE Trans Power Appar Syst.* 1984;PAS-103(5):1045-1051.

https://doi.org/ 10.1109/tpas.1984.318710

54. Wu FF, Dea VS. Describing-function analysis of automatic generation control system with governor deadband. *Electr Power Syst Res.* 1978;1(2):113-116.

https://doi.org/ 10.1016/0378-7796(78)90003-2

55. Tripathy SC, Hope GS, Malik OP. Optimisation of load-frequency control parameters for power systems with reheat steam turbines and governor deadband nonlinearity. *IEE Proc C Gener Transm Distrib UK*. 1982;129(1):10.

https://doi.org/ 10.1049/ip-c.1982.0002

56. Patra KC, Patnaik A. Research on stabilizing and eliminating limit cycles in 3D nonlinear systems characterized by hysteresis. *Int J Appl Math Comput Sci Syst Eng*. 2025;7:214-239.

https://doi.org/ 10.37394/232026.2025.7.19

57. Sea RG, Vacroux AG. Steady state analysis of non-linear systems and multiple input describing functions (M.I.D.F.). *Automatica*. 1969;5(6):763-772.

https://doi.org/ 10.1016/0005-1098(69)90089-2

58. Atherton DP, Towill DR. Nonlinear Control Engineering-Describing Function Analysis and Design. *IEEE Trans Syst Man Cybern.* 1977;7(9):678.

https://doi.org/ 10.1109/tsmc.1977.4309808

59. Benjamin CK, Zoss LM. *Digital Control Systems*, Oxford: Oxford University Press, 2nd Edition, 8th Impression; 2009.

60. Patra KC, Patnaik A. Estimation of Limit Cycles and Signal Stabilization with Deadbeat approach in three Dimensional Nonlinear systems. *Int J Control Syst Robot.* 2025;10:22-38.

61. Patra KC, Patnaik A. Load Frequency Control by Speed Governors of Two-Area Power System using Digital Controller with Deadbeat Approach. *Int J Electr Eng Comput Sci.* 2025;7:200-217.

https://doi.org/ 10.37394/232027.2025.7.19

62. Nasab MA, Al-Shibli WK, Zand M, Ehsan-Maleki B, Padmanaban S. Charging management of electric vehicles with the presence of renewable resources. *Renew Energy Focus.* 2024;48:100536.

https://doi.org/ 10.1016/j.ref.2023.100536

Appendix

Table A1. Model parameters used for the load frequency control **system**

Parameters	**Value**
Governor speed regulation parameter	0.417
Power system gain	0.01–1
Steam turbine time constant	0.3–0.5 s
Steam turbine reheat time constant	10 s
Governor time constant	0.08 s
Droop compensation time constant	28.75 s